

Accessing extended and partially fused hexabenzocoronenes using a benzannulation–cyclodehydrogenation approach†

Cite this: DOI: 10.1039/c3sc51212f

Hasan Arslan, Fernando J. Uribe-Romo, Brian J. Smith and William R. Dichtel*

A rapid and efficient approach to prepare extended or partially fused hexabenzocoronene derivatives is described. The method is based on the sequential benzannulation and cyclodehydrogenation (Scholl oxidation) of simple diaryl alkynes. The benzannulation reaction proceeds efficiently on highly congested substrates and with complete regioselectivity. Scholl oxidation of the resulting oligo(arylene)s proceeds without rearrangements and provides either fully fused or specific partially fused polycyclic aromatic hydrocarbon products. The partially fused derivatives are a new class of contorted aromatic systems with high solubility, enhanced visible absorption, and reversible redox processes. The efficiency and specificity of the benzannulation and oxidation reactions are promising for accessing new classes of organic semiconductors and carbon nanostructures.

Received 3rd May 2013
Accepted 10th July 2013

DOI: 10.1039/c3sc51212f

www.rsc.org/chemicalscience

Extended polycyclic aromatic hydrocarbons (PAHs),^{1–4} such as the hexabenzocoronenes (HBCs), are functional π -electron systems whose desirable optical and electronic properties have attracted interest for organic thin film transistor (OTFT)^{5–7} and organic photovoltaic (OPV) devices.^{8,9} The device properties of specific PAHs depend both on their electronic structure and packing behaviour. The nature of these assemblies is influenced by molecular shape, the position and identity of solubilizing groups, molecule–substrate interactions, and processing methods used to form thin films. For example, Müllen and coworkers have made major contributions to both the synthesis of novel HBC derivatives and their solid-state organization.^{10–12} Other instructive examples of the interplay between HBC structure and long-range order that produce emergent properties include nanotubes derived from amphiphilic HBCs studied by Aida^{13–15} and contorted HBCs studied by Nuckolls^{16–25} and Miao²⁶ for OTFTs and OPVs.

Efficient and convergent syntheses of HBCs with novel substitution patterns, extended conjugation, or nonplanar structures will allow their full potential to be realized. Less symmetric substitution patterns, such as those of interest for amphiphilic derivatives, can require laborious syntheses, while introducing additional fused rings confers lower HOMO–LUMO gaps and can induce curvature. Here we introduce a new strategy to access HBC derivatives by benzannulating readily accessible diarylalkynes. We recently demonstrated the high

efficiency of this transformation to convert the alkyne functions of a poly(phenylene ethynylene) (PPE) into 2,3-diaryl-naphthalene moieties.²⁷ The reaction tolerates aryl substituents adjacent to the alkynes, a promising feature for PAH synthesis provided that the resulting oligoarylenes can be cyclodehydrogenated efficiently and without rearrangements.

Substituted diarylalkyne derivatives **1a–d** are ideal substrates to evaluate the benzannulation–cyclodehydrogenation approach for PAH synthesis (Fig. 1). This strategy provides HBC derivatives with extended conjugation and complementary substitution patterns relative to existing methods. Here we show that the benzannulation reaction is efficient for several HBC precursors and that typical Scholl oxidation conditions do

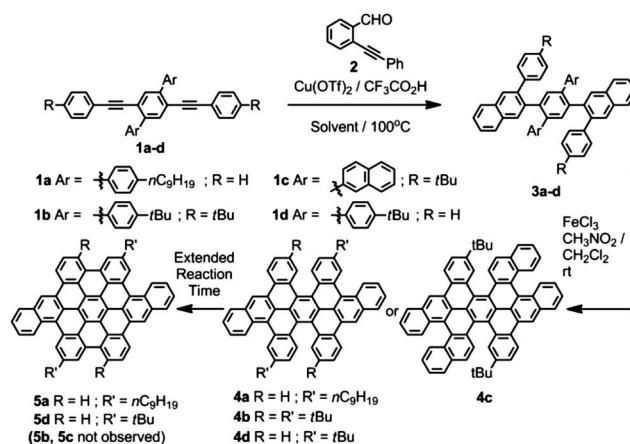


Fig. 1 A series of dialkyne compounds **1a–d** provide partially fused HBC derivatives **4a–d** and fully fused products **5a** and **5d** using a two-step benzannulation–cyclodehydrogenation protocol.

Baker Laboratory, Department of Chemistry and Chemical Biology, Cornell University, Ithaca, NY 14853-1301, USA. E-mail: wdichtel@cornell.edu

† Electronic supplementary information (ESI) available: Experimental procedures and characterization data for all reported compounds and precursors. See DOI: 10.1039/c3sc51212f

not induce rearrangements. In some cases, complete cyclohydrogenation is achieved; however, shorter reaction times or strategically placed substituents provide partially fused products. When complete oxidation does not occur, the order of carbon-carbon bond formation is well defined, providing specific, non-planar coronene derivatives **4a-c** that exhibit high solubility, strong visible absorption, and reversible redox processes. Collectively, these molecular compounds also represent important model systems for oxidizing benzannulated PPEs to produce structurally precise graphene nanoribbons, and their lack of rearrangements show great promise in this regard.

We evaluated the generality and efficiency of the benzannulation reaction across several substituted di(arylethynyl)-benzene derivatives. The di(*n*-nonyl)terphenyl compound **1a** is a molecular analogue of the repeat unit of our previously reported PPE system²⁷ that was benzannulated in the presence of 2-(phenylethynyl)benzaldehyde, Cu(OTf)₂, and CF₃CO₂H. Similar conditions provide the oligoarylene **3a** in 98% isolated yield. We also evaluated dialkynes **1b** and **1d**, which have four and two peripheral *t*-butyl substituents, respectively. The *t*Bu groups serve three primary functions: (1) they are effective solubilizing groups for PAHs; (2) they are convenient and sensitive NMR handles for rapidly diagnosing side reactions and rearrangements; and (3) oxidation of *t*Bu-substituted substrates often do not fuse completely because of steric hindrance.²⁸ Such partially oxidized products offer unique properties associated with their non-planar structures as well as insight into the sequence of C-C bond forming steps of fully fused systems. Finally, we evaluated compound **1c**, which has 2-naphthyl groups as central aryl substituents. This compound provides access to larger fused aromatic systems and serves as a model for a benzannulated polymer that might provide a graphene nanoribbon with an armchair edge structure. Dialkynes **1b-d** were each benzannulated in similarly high efficiency based on analysis of their crude reaction mixtures.

We also benzannulated **1a** with isotopically labelled benzaldehyde 2-¹³C₂ (Fig. 2). The resulting benzannulated product **3a-¹³C₂** contained one isotopic label per reactive site, as determined by mass spectroscopy, ¹³C NMR spectroscopy (Fig. 2b), and a full complement of 2D NMR spectroscopy experiments (Fig. S24 and S44-S51 in the ESI†). The incorporation of a single isotopic label at these positions is consistent with Yamamoto's proposed mechanism²⁹ with the regioselectivity indicated in Fig. 2c, while the other ¹³C label is eliminated upon aromatization of the newly formed naphthalene. This regioselectivity might derive from the formal [4 + 2] cycloaddition occurring in a stepwise manner, in which the first new carbon-carbon σ bond is formed between the less hindered alkyne carbon and the oxonium carbon of the benzopyrylium intermediate. The regioselectivity of the benzannulation reaction, combined with isotopic labelling, offer a powerful means to characterize Scholl oxidation products. These findings also suggest that non-symmetric derivatives of **2** will provide PAHs with specifically placed substituents.

Dinonyl derivative **3a** was cyclodehydrogenated using FeCl₃. MALDI-TOF mass spectrum of the reaction mixture after 1 h

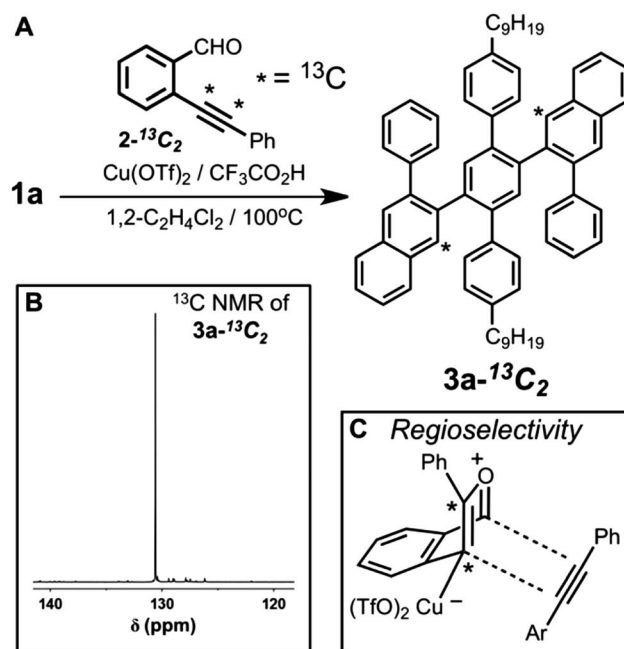


Fig. 2 (A) The benzannulation of **1a** with 2-¹³C₂ provides the labelled derivative **3a-¹³C₂**, indicating that the reaction is regioselective. (B) Partial ¹³C NMR of **3a-¹³C₂**. (C) Regiochemistry of the benzannulation reaction consistent with this experiment.

indicated a loss of 12 amu, corresponding to the formation of 6 C-C bonds and complete fusion of the coronene core. Although ¹H and ¹³C NMR spectroscopy of **5a** were consistent with the expected structure, the low solubility and propensity of this compound to aggregate complicated its definitive structural characterization. Furthermore, King *et al.* noted rearrangements in a closely related system that had been misassigned in the literature for many years (Fig. 3).³⁰ Therefore, we prepared several additional model compounds that would exhibit improved solubility to enable unambiguous characterization of the fused PAHs. These model systems incorporate 4'-*t*Buphenyl substituents, as well as variations of the central arylene group.

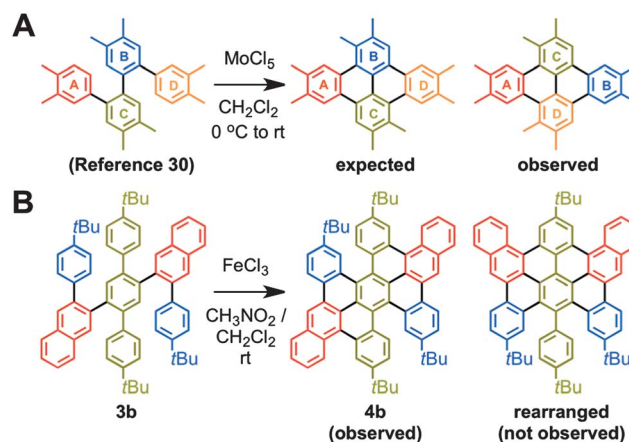


Fig. 3 (A) Rearrangement during the Scholl oxidation observed by King *et al.*³⁰ (B) The expected (observed) and possible rearranged (not observed) products for the oxidation of **3b**.

In order to investigate the possibility of rearrangements during the oxidation, we subjected **3b** to the same Scholl oxidation conditions. By incorporating the *t*Bu groups on the central terphenyl and external phenyl groups, **3b** does not fuse completely. MALDI-TOF MS indicated a reduction in mass of 8 amu, corresponding to the formation of four of the six expected C–C bonds. The ^1H NMR spectrum of **4b** provides unambiguous evidence that 1,2-aryne rearrangements observed in other systems do not occur (Fig. 4). For example, two singlets corresponding to *t*Bu resonances are observed at 1.46 and 1.25 ppm, respectively, which integrate to a 1 : 1 ratio. The analogous rearrangement to that reported by King and coworkers would instead provide a compound with three *t*Bu resonances in a 1 : 2 : 1 integration ratio (Fig. 3b). The aromatic region of the ^1H NMR spectrum of **4b** indicates the formation of the non-rearranged but partially fused structure depicted in Fig. 4. Eleven aromatic resonances are observed, rather than nine expected for the fully fused compound. A complete assignment of the spectrum using complementary 2D NMR experiments (COSY, ROESY, HSQC and HMBC; see Section D in the ESI†) indicates that C–C bonds between the *t*Bu functionalized aromatic rings do not form. We hypothesize that steric hindrance associated with these groups causes distortions from planarity that prevent these final two C–C bonds from forming. The ROESY spectrum of **4b** is consistent with this hypothesis, as clear cross peaks are observed between H_c and H_b (7 bonds apart) and H_j and H_k (6 bonds apart) in addition to those between adjacent hydrogen atoms on the periphery. A derivative that contains central 2-naphthyl substituents (**3c**), also partially fuses under the oxidation conditions. MALDI-TOF MS indicated the formation of four C–C bonds. The regiochemistry of bond formation was unambiguously characterized by NMR spectroscopy. Interestingly, only one C–C bond was formed between

each pair of adjacent naphthalene systems, which we also attribute to steric interactions associated with the *t*Bu groups.

We next analyzed the reaction mixtures of various Scholl oxidations as a function of reaction time and gained insight into the order and relative rates of C–C bond formation within these benzannulated compounds. We first characterized the oxidation of compound **3d**, which retains the two 4-*t*Bu phenyl substituents on the central aromatic ring but lacks the external *t*Bu groups of compound **3b**. Prior to FeCl_3 addition, **3d** exhibits an isotopically resolved MALDI-TOF mass spectrum corresponding to its expected mass (Fig. 5, $t = 0$). A spectrum of the reaction mixture recorded 20 min after adding the oxidant exhibits its most intense peak eight mass units lower, corresponding to the formation of four new C–C bonds. No peaks are observed for species of intermediate mass between **3d** and this partially fused intermediate, and low intensity signals 1–4 amu lower than the main peak correspond to further fused products. At 60 min, these peaks increase in intensity, and the mass spectrum indicates essentially complete formation of **5d** at

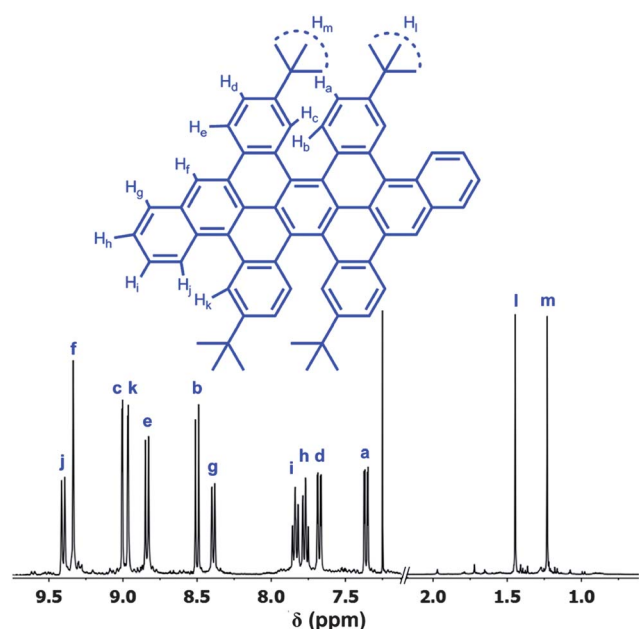


Fig. 4 Partial ^1H NMR spectrum of the aromatic and *t*Bu regions of **4b**.

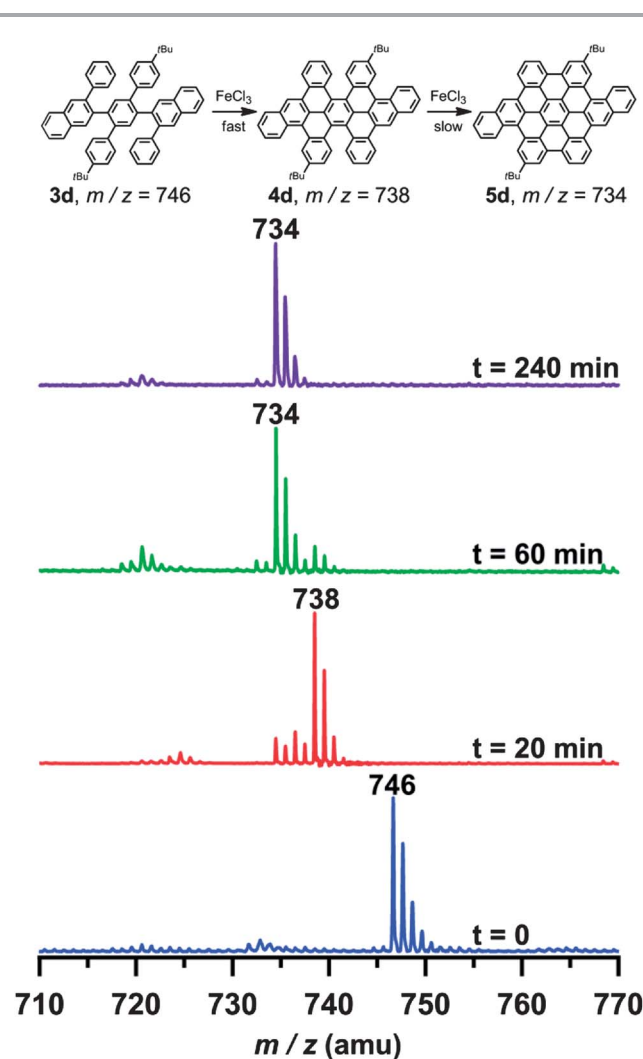


Fig. 5 MALDI-TOF MS spectra taken of the oxidation of **3d** as a function of reaction time. Four carbon–carbon bonds are formed in fewer than 20 minutes, while full oxidation occurs after longer reaction times.

240 min. By analogy to **4b**, in which the final two C–C bonds do not form even at extended reaction times, we hypothesized that the four C–C bonds formed rapidly in **4d** correspond to those present in **4b**. This hypothesis is further supported by a similar study of the oxidation of the di-*n*-nonyl functionalized compound **3a**. MALDI-TOF MS of the oxidation of **3a** at $t = 5$ min also indicated formation of an intermediate oxidation product containing the first four C–C bonds, followed by complete oxidation at longer reaction times. We stopped a preparative scale oxidation of **3a** after 5 min and isolated the partially oxidized product, which was highly soluble in many organic solvents. ^1H NMR analysis indicated twelve resolved aromatic resonances consistent with the structure **4a** (Sections C and D in the ESI†). Interestingly, partial fusion of a related *o*-phenylene containing systems was observed by Müllen³¹ and Moore.³² However, a different regiochemistry (order of bond formation) was observed. A comparison of these results suggests that the course of the Scholl oxidation is highly sensitive to subtle changes in structure.

The partially fused systems are nonplanar PAHs, as indicated by calculating their structures using Density Functional Theory (DFT). We optimized the geometries of **4a–d** and **5a–d** (for **4a** and **5a**, the *n*-nonyl chains were truncated to methyl groups). Each of the partially fused structures **4a–d** show significant distortion from planarity, in which the dihedral torsion angle at the site of final cyclodehydrogenation is 56° (Fig. 6 and Fig. S86 in the ESI†). For compound **4a**, we considered two possible conformations, namely twisted (Fig. 6) and anti (Fig. S87 in the ESI†). The two structures are energetically similar, with the twisted conformation predicted to be $0.9 \text{ kcal mol}^{-1}$ more stable in the gas phase, and both structures exhibit large deviations from planarity. Their barrier to interconversion is high ($>20 \text{ kcal mol}^{-1}$), and only a single conformation of **4a** was

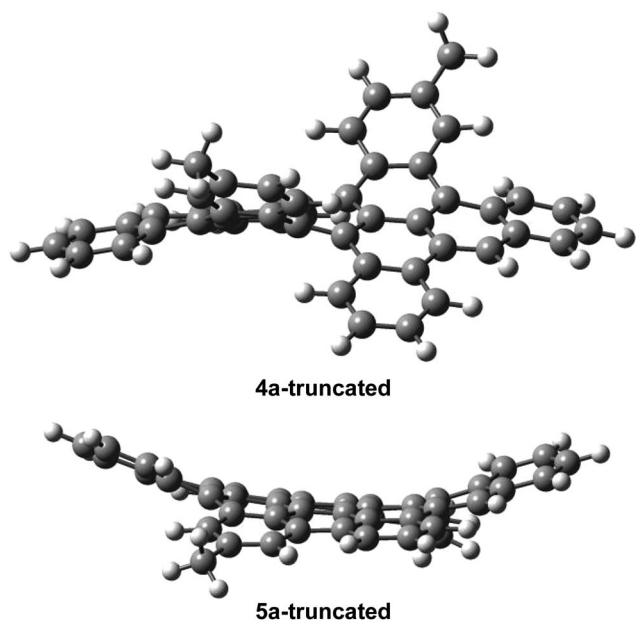


Fig. 6 DFT-optimized structures of partially and fully fused compounds **4a** and **5a**, respectively. The $n\text{-C}_9\text{H}_{19}$ chains were truncated to $-\text{CH}_3$ groups in the calculations.

observed by NMR spectroscopy. Although both structures are viable, we predict that **4a** adopts the twisted form based on previous work with a similar contorted compound²⁶ and the limited conformational freedom of precursor **3a**. In contrast, fully fused compounds **5a** and **5d** are nearly planar ($2\text{--}3^\circ$ dihedral angle). For **5b** and **5c**, which were not observed experimentally, the internal arene torsion of the optimized structure is $10\text{--}11^\circ$, suggesting that the strain of forming the final carbon–carbon bonds precludes complete fusion of these compounds.

Contorted HBCs have attracted interest for their shape complementarity to fullerenes and distinct optical and electronic properties. For example, HBCs are typically yellow compounds, whereas solutions of **4a** and **4b** are orange and those of **4c** are red. UV/vis spectroscopy indicated similar spectra for each compound, with significant absorption bands in the $450\text{--}550 \text{ nm}$ range and molar absorptivity $\geq 20\,000 \text{ M}^{-1} \text{ cm}^{-1}$ (Fig. 7a). The absorption onsets of each compound, from which the optical HOMO–LUMO gaps are determined, are $\sim 540 \text{ nm}$ for **4a** and **4b** and 575 nm for the more extended derivative **4c**. These onsets correspond to optical HOMO–LUMO gaps of 2.32 eV for both **4a** and **4b** and 2.16 eV for **4c** (these optical and electrochemical HOMO–LUMO gaps are collected in Table S3 in the ESI†). For all structures analyzed computationally, both the HOMO and LUMO are delocalized across the molecule, consistent with a small Stokes shift (see Table S1 in the ESI†). The DFT calculated HOMO–LUMO gaps trend is consistent with the experimental values (2.72 eV , 2.76 eV , and 2.60 eV for **4a**, **4b**, and **4c**, respectively). The lowest energy optical transition of **4a** is influenced by its nonplanar structure, as evidenced by the spectrum of the corresponding fully fused derivative **5a**, which does not absorb strongly in this region (Fig. S84 in the ESI†). A contorted PAH most similar in structure to the aromatic core of **4a–c** exhibits similar absorbance and fluorescence properties,³³ and these effects on the absorbance of nonplanar coronene derivatives were also noted by Nuckolls and coworkers.²³ Each compound is strongly fluorescent, and **4a** and **4b** have nearly identical photoemission spectra with λ_{max} at 505 nm (Fig. 7b). The emission of **4c** has a very similar peak shape and λ_{max} of 540 nm . These maximum emission wavelengths correspond to low Stokes shifts ($\sim 25 \text{ nm}$) for each compound that are consistent with their expected rigid structures. The partially fused derivatives described here maintain reasonable fluorescence quantum yield, whereas nonplanarity induced by incorporating five-membered rings into similar systems was accompanied by dramatic reductions in their quantum yield.²³

Electrochemical studies provided additional insight into the redox processes and energy levels of the partially fused compounds (Fig. 8). Cyclic voltammetry of **4a–c** was performed in $0.1 \text{ M Bu}_4\text{NPF}_6$ in CH_2Cl_2 on a Pt button electrode, with potentials reported relative to the ferrocene/ferrocenium (Fc/Fc^+) redox couple. **4a** and **4b** exhibit two electrochemically irreversible but chemically reversible oxidation processes, each with a first onset potential of 0.22 V . The corresponding oxidation processes are also observed for **4c** at similar onset potentials of 0.24 V . Differences in the reduction processes of these compounds are more pronounced. **4a** and **4b** are reduced

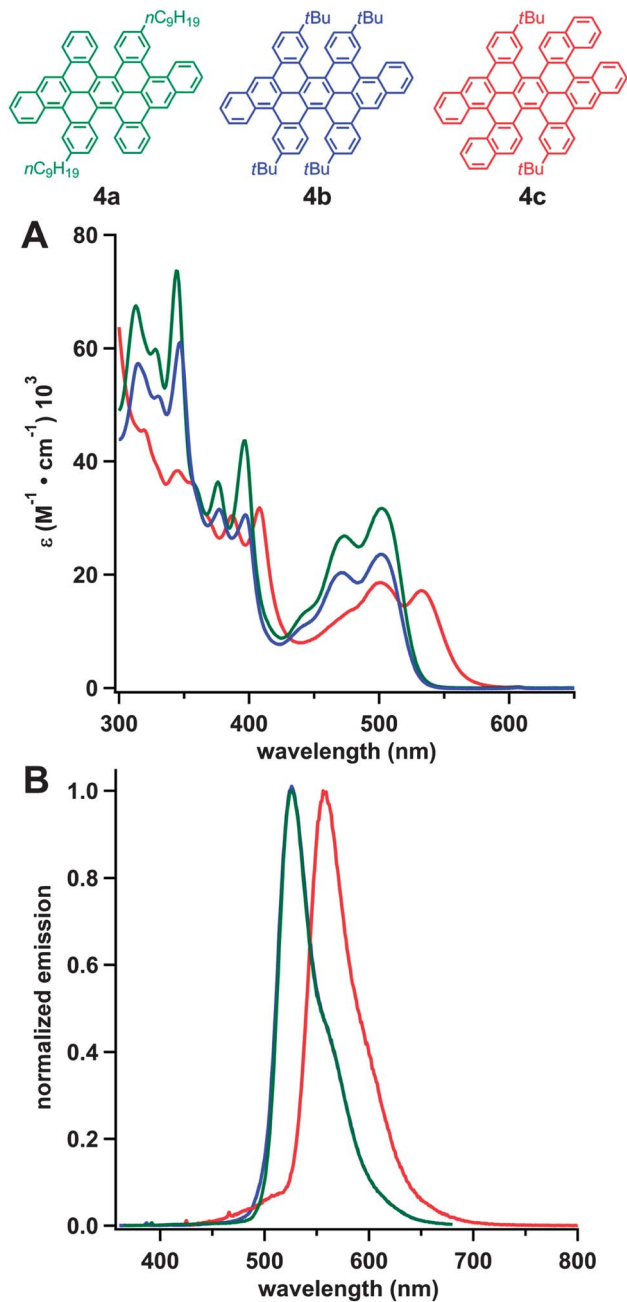


Fig. 7 (A) UV-vis and (B) fluorescence spectra of contorted compounds **4a-c**.

at onset potentials of -1.79 and -1.80 V, respectively. The reduction of **4a** is chemically reversible, whereas the reduction of **4b** is chemically irreversible and may correspond to a multi-electron reduction process. The reduction of **4c** occurs at a less negative potential of -1.57 V and is also chemically irreversible. These measurements give rise to electrochemical HOMO-LUMO gaps of 2.01, 2.02, and 1.81 eV for **4a-c**, respectively, which correspond reasonably well to those determined optically. In contrast, CV of a film of the fully fused derivative **5a**- $^{13}\text{C}_2$ cast on a Pt button working electrode exhibited no reduction processes at potentials > -2.2 V. The oxidation onset of these films is at 0.40 V, 0.18 V more positive than **4a** and is

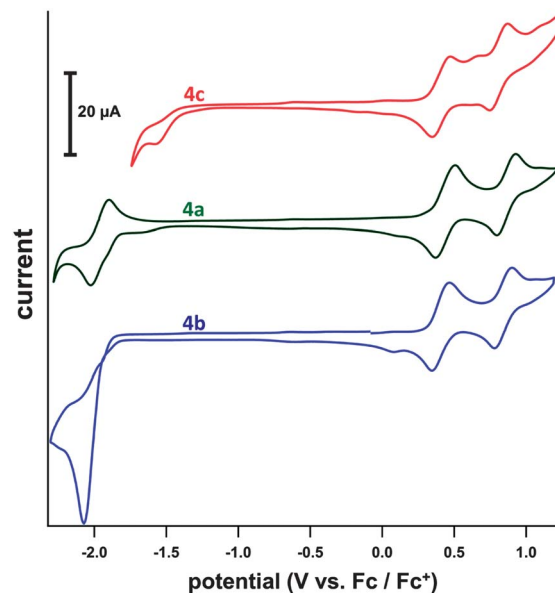


Fig. 8 Cyclic voltammetry (0.1 M Bu_4NPF_6 in CH_2Cl_2 ; Pt button electrode) of **4a-c**.

chemically irreversible (Fig. S87 in the ESI †). Overall, the similar oxidation potentials of each compound, along with the shift in the reduction potential of **4c** relative to **4a** and **4b** suggest that the extended conjugation of **4c** predominantly lowers its LUMO energy, making it a better electron acceptor.

Conclusions

We have demonstrated a sequential benzannulation-cyclodehydrogenation strategy to access new PAH architectures from easily prepared arylene ethynyls. This approach provides efficient access to both fully fused and partially fused hexabenzocoronene derivatives with extended conjugation and differing substitution patterns than those available from existing methods. Rearranged products were not observed under these conditions. The partially fused derivatives are underexplored and feature high solubility, increased absorptivity in the visible spectrum, and reversible redox processes. The high efficiency of the benzannulation reaction shows great promise for synthesizing other novel PAH systems. The benzannulated derivatives explored here are also important models for accessing graphene nanoribbons by applying the benzannulation-cyclodehydrogenation approach to appropriately substituted PPEs. This study confirms the promise of such an approach in that no rearrangements were observed in the Scholl oxidation step, although complete fusion in the polymer systems should be demonstrated carefully. We will next apply these methods to access new carbon nanostructures and other aromatic systems.

Acknowledgements

This work was supported by the Beckman Young Investigator Program of the Arnold and Mabel Beckman Foundation, the NSF

(CHE-1124754), the Doctoral New Investigator Program of the ACS Petroleum Research Fund (52019-DNI7), the Cottrell Scholar Program of the Research Corporation for Science Advancement, and a Sloan Research Fellowship from the Alfred P. Sloan Foundation. This work made use of the Cornell Center for Materials Research Facilities supported by the National Science Foundation under Award Number DMR-1120296. We acknowledge Dr Ivan Keresztes for assistance with NMR spectroscopy.

References

- 1 S. Pogodin and I. Agranat, *Org. Lett.*, 1999, **1**, 1387–1390.
- 2 L. T. Scott, *Pure Appl. Chem.*, 1996, **68**, 291–300.
- 3 A. C. Grimsdale and K. Müllen, *Angew. Chem., Int. Ed.*, 2005, **44**, 5592–5629.
- 4 B. Hajgató, M. S. Deleuze and K. Ohno, *Chem.–Eur. J.*, 2006, **12**, 5757–5769.
- 5 S. R. Forrest, *Nature*, 2004, **428**, 911–918.
- 6 C. D. Dimitrakopoulos and P. R. L. Malenfant, *Adv. Mater.*, 2002, **14**, 99–117.
- 7 X. Guo, M. Myers, S. Xiao, M. Lefenfeld, R. Steiner, G. S. Tulevski, J. Tang, J. Baumert, F. Leibfarth, J. T. Yardley, M. L. Steigerwald, P. Kim and C. Nuckolls, *Proc. Natl. Acad. Sci. U. S. A.*, 2006, **103**, 11452–11456.
- 8 C. Li, M. Liu, N. G. Pschirer, M. Baumgarten and K. Müllen, *Chem. Rev.*, 2010, **110**, 6817–6855.
- 9 L. Schmidt-Mende, A. Fechtenkötter, K. Müllen, E. Moons, R. H. Friend and J. D. MacKenzie, *Science*, 2001, **293**, 1119–1122.
- 10 T. M. Figueira-Duarte and K. Müllen, *Chem. Rev.*, 2011, **111**, 7260–7314.
- 11 W. Pisula, X. Feng and K. Müllen, *Chem. Mater.*, 2011, **23**, 554–567.
- 12 B. Schmaltz, T. Weil and K. Müllen, *Adv. Mater.*, 2009, **21**, 1067–1078.
- 13 J. P. Hill, W. S. Jin, A. Kosaka, T. Fukushima, H. Ichihara, T. Shimomura, K. Ito, T. Hashizume, N. Ishii and T. Aida, *Science*, 2004, **304**, 1481–1483.
- 14 W. Jin, T. Fukushima, M. Niki, A. Kosaka, N. Ishii and T. Aida, *Proc. Natl. Acad. Sci. U. S. A.*, 2005, **102**, 10801–10806.
- 15 Y. Yamamoto, T. Fukushima, Y. Suna, N. Ishii, A. Saeki, S. Seki, S. Tagawa, M. Taniguchi, T. Kawai and T. Aida, *Science*, 2006, **314**, 1761–1764.
- 16 C.-Y. Chiu, B. Kim, A. A. Gorodetsky, W. Sattler, S. Wei, A. Sattler, M. Steigerwald and C. Nuckolls, *Chem. Sci.*, 2011, **2**, 1480–1486.
- 17 Y. S. Cohen, S. Xiao, M. L. Steigerwald, C. Nuckolls and C. R. Kagan, *Nano Lett.*, 2006, **6**, 2838–2841.
- 18 A. M. Hiszpanski, S. S. Lee, H. Wang, A. R. Woll, C. Nuckolls and Y.-L. Loo, *ACS Nano*, 2013, **7**, 294–300.
- 19 S. J. Kang, S. Ahn, J. B. Kim, C. Schenck, A. M. Hiszpanski, S. Oh, T. Schiros, Y.-L. Loo and C. Nuckolls, *J. Am. Chem. Soc.*, 2013, **135**, 2207–2212.
- 20 S. J. Kang, J. B. Kim, C.-Y. Chiu, S. Ahn, T. Schiros, S. S. Lee, K. G. Yager, M. F. Toney, Y.-L. Loo and C. Nuckolls, *Angew. Chem., Int. Ed.*, 2012, **51**, 8594–8597.
- 21 Y.-L. Loo, A. M. Hiszpanski, B. Kim, S. Wei, C.-Y. Chiu, M. L. Steigerwald and C. Nuckolls, *Org. Lett.*, 2010, **12**, 4840–4843.
- 22 K. N. Plunkett, K. Godula, C. Nuckolls, N. Tremblay, A. C. Whalley and S. Xiao, *Org. Lett.*, 2009, **11**, 2225–2228.
- 23 A. C. Whalley, K. N. Plunkett, A. A. Gorodetsky, C. L. Schenck, C.-Y. Chiu, M. L. Steigerwald and C. Nuckolls, *Chem. Sci.*, 2011, **2**, 132–135.
- 24 S. X. Xiao, M. Myers, Q. Miao, S. Sanaur, K. L. Pang, M. L. Steigerwald and C. Nuckolls, *Angew. Chem., Int. Ed.*, 2005, **44**, 7390–7394.
- 25 S. Xiao, S. J. Kang, Y. Wu, S. Ahn, J. B. Kim, Y.-L. Loo, T. Siegrist, M. L. Steigerwald, H. Li and C. Nuckolls, *Chem. Sci.*, 2013, **4**, 2018–2023.
- 26 J. Luo, X. Xu, R. Mao and Q. Miao, *J. Am. Chem. Soc.*, 2012, **134**, 13796–13803.
- 27 H. Arslan, J. D. Saathoff, D. N. Bunck, P. Clancy and W. R. Dichtel, *Angew. Chem., Int. Ed.*, 2012, **51**, 12051–12054.
- 28 A. Pradhan, P. Dechambenoit, H. Bock and F. Durola, *Angew. Chem., Int. Ed.*, 2011, **50**, 12582–12585.
- 29 N. Asao, T. Nogami, S. Lee and Y. Yamamoto, *J. Am. Chem. Soc.*, 2003, **125**, 10921–10925.
- 30 J. L. Ormsby, T. D. Black, C. L. Hilton, Bharat and B. T. King, *Tetrahedron*, 2008, **64**, 11370–11378.
- 31 X. Feng, J. Wu, V. Enkelmann and K. Müllen, *Org. Lett.*, 2006, **8**, 1145–1148.
- 32 Y. Lu and J. S. Moore, *Tetrahedron Lett.*, 2009, **50**, 4071–4077.
- 33 Y. Fujimaki, M. Takekawa, S. Fujisawa, S. Ohshima and Y. Sakamoto, *Polycyclic Aromat. Compd.*, 2004, **24**, 107–122.